Mobility of Cytoplasmic, Membrane, and DNA-Binding Proteins in *Escherichia coli*

Mohit Kumar,[†△] Mario S. Mommer,[‡△] and Victor Sourjik[†*]
[†]Zentrum für Molekulare Biologie der Universität Heidelberg, DKFZ-ZMBH Alliance, Heidelberg, Germany; and [‡]Interdisziplinäres Zentrum für Wissenschaftliches Rechnen, Universität Heidelberg, Heidelberg, Germany

ABSTRACT Protein mobility affects most cellular processes, such as the rates of enzymatic reactions, signal transduction, and assembly of macromolecular complexes. Despite such importance, little systematic information is available about protein diffusion inside bacterial cells. Here we combined fluorescence recovery after photobleaching with numerical modeling to analyze mobility of a set of fluorescent protein fusions in the bacterial cytoplasm, the plasma membrane, and in the nucleoid. Estimated diffusion coefficients of cytoplasmic and membrane proteins show steep dependence on the size and on the number of transmembrane helices, respectively. Protein diffusion in both compartments is thus apparently obstructed by a network of obstacles, creating the so-called molecular sieving effect. These obstructing networks themselves, however, appear to be dynamic and allow a slow and nearly size-independent movement of large proteins and complexes. The obtained dependencies of protein mobility on the molecular mass and the number of transmembrane helices can be used as a reference to predict diffusion rates of proteins in *Escherichia coli*. Mobility of DNA-binding proteins apparently mainly depends on their binding specificity, with FRAP recovery kinetics being slower for the highly specific TetR repressor than for the relatively nonspecific H-NS regulator.

INTRODUCTION

Protein mobility is one of the key parameters in the quantitative description of cellular processes. In the cell, diffusion largely defines the upper rate limit of biochemical reactions, in addition to the rate of responses to extracellular stimuli. It is particularly important in bacteria, which apparently lack active mechanisms of protein transport and therefore have to rely on passive delivery of proteins and even large protein complexes to their target sites. Despite such importance for a quantitative description of cellular processes, only limited information is available on the diffusional properties of the bacterial cytoplasm, the plasma membrane, or the nucleoid. Previous studies analyzed diffusion of only a few selected proteins in bacteria (1–4), and also differed in the experimental approach, data evaluation, model bacterial system, and growth conditions—making it difficult to draw general conclusions about dependence of mobility on protein size and other properties.

Here we used fluorescence recovery after photobleaching (FRAP) along with a detailed numerical model that simulates FRAP experiments, to systematically investigate mobility of cytoplasmic, inner membrane, and DNA-binding proteins in *Escherichia coli*. Our data confirm the view of the cytoplasm as a molecular sieve, with a steep dependence of diffusion coefficient on the protein size, and also suggest a dynamic nature of this sieve that allows slow and nearly size-independent diffusion of large proteins. The obtained dependencies of protein mobility on the molecular mass and the number of transmembrane helices can be used as a reference to predict the diffusion rate of a particular protein in *E. coli*.

MATERIALS AND METHODS

Experimental methods

Bacterial strains and plasmids

All experiments with cytoplasmic and membrane protein fusions were performed in *E. coli* K-12 strain RP437 (5) or in its Δ*flhC* derivative VS116 (6). The experiments with the H-NS fusion were performed in strain MG1655 and the experiments with the TetR-YFP fusion were performed in strain SR1, a RP437 derivative carrying *tetO* array near the replication origin (7). Fusions to the A206K mutant of the enhanced yellow fluorescent protein (YFP) were expressed under the control of a pTrc promoter (8), which is inducible by isopropyl-β-D-thiogalactopyranoside. Optimal levels of induction for individual constructs were determined by a visual microscopic examination. The extent of degradation of fusion proteins was accessed using immunoblotting with monoclonal anti-GFP antibody (Sigma, St. Louis, MO). All fusions and their degree of degradation are summarized in Table 1 and plasmids with corresponding induction levels and background strains are summarized in Table S1 in the Supporting Material.

Cell growth and preparation

Overnight cultures were grown at 30°C in 5 mL tryptone broth (10 g/L tryptone, 5 g/L NaCl, pH 7.0) containing 100 μg/mL ampicillin. Daily cultures were prepared by diluting the overnight culture 1:100 in 10 mL tryptone broth containing 100 μg/mL ampicillin and the appropriate concentration of isopropyl-β-D-thiogalactopyranoside (Table S1). The cultures were exposed to 1% cephalexin (w/v) after 3 h of induction at 34°C and 275 rpm, and were harvested after 3.5 h (except for the MG1655 strain, which was allowed to grow for 4 h). After harvesting, the cells were washed once with tethering buffer (10 mM KH_2PO_4/K_2HPO_4, 0.1 mM EDTA; 10 mM sodium lactate, 67 mM NaCl, 1 μM methionine, pH 7.0), and resuspended in 10 mL tethering buffer. Before FRAP experiments, cells were incubated in buffer for at least 30 min at room temperature to ensure the full maturation of fluorescent proteins, and were subsequently immobilized on poly-L-lysine-coated coverslips for 5 min.

Submitted April 16, 2009, and accepted for publication November 2, 2009.

△Mohit Kumar and Mario S. Mommer equally contributed to this work.

*Correspondence: v.sourjik@zmbh.uni-heidelberg.de

Editor: George Barisas.

0006-3495/10/02/0552/8 $2.00

doi: 10.1016/j.bpj.2009.11.002

TABLE 1 Summary of FRAP experiments and model fit parameters

Protein fusion	Physiological role	MM (kDa)	TM domains	pI	Degree of degradation	No. of exp.	Cell length (μm) ± SD	Apparent diffusion coefficient ($\mu m^2/s$) ± $CI_{95\%}$*	Mobile fraction
Cytoplasmic fusions									
eYFP	—	26.7	—	5.72	100% (26.7 kDa)	95	5.03 ± 0.73	7.08 ± 0.32	0.99
PtsH-YFP	Phospho-carrier protein; sugar phosphotransferase system	35.8	—	5.69	84% (35.8 kDa) 16% (26.7 kDa)	79	4.70 ± 0.73	3.78 ± 0.16	0.99
Crr-YFP	Component of glucose-specific phosphotransferase enzyme IIA	45.0	—	5.17	96% (45 kDa) 4% (26.7 kDa)	113	4.97 ± 0.75	2.03 ± 0.05	0.97
CFP-CheW-YFP	Chemotaxis protein	71.5	—	5.21	69.5% (71.5 kDa) 13% (~55 kDa) 14.5% (~43kDa) 3% (26.7 kDa)	96	4.49 ± 0.73	1.51 ± 0.05	0.96
CFP-CheR-YFP	Chemotaxis protein methyltransferase	86.2	—	6.38	82% (86.2 kDa) 18% (70 kDa)	97	4.19 ± 0.72	1.70 ± 0.05	0.96
DnaK-YFP	Molecular chaperone	95.8	—	5.10	70% (95.8 kDa) 30% (26.7 kDa)	99	5.32 ± 0.80	0.67 ± 0.02	0.96
HtpG-YFP	Molecular chaperone	198.0†	—	5.22	~100% (2 × 99 kDa)	40	4.96 ± 0.87	1.65 ± 0.07	0.99
CFP-CheA-YFP	Chemotaxis protein	249.6†	—	5.10	44% (249.6 kDa) 40% (~2 × 100 kDa) 6% (~2 × 60 kDa) 10% (26.7 kDa)	36	5.04 ± 1.03	0.44 ± 0.06	0.90
Membrane-bound fusions									
Tar(1-397)-YFP	Fragment of the aspartate chemoreceptor	142.3†	4	5.90	—	8	4.46 ± 1.00	0.217 ± 0.030	0.98
Tsr(1-218)-YFP	Fragment of the serine chemoreceptor	102.2†	4	5.82	—	12	5.21 ± 0.82	0.182 ± 0.016	0.98
LacY-YFP	Lactose permease	73.2	12	7.18	—	9	4.81 ± 0.70	0.0265 ± 0.0034	0.97
MtlA-YFP	Mannitol-specific EIICBA of the phosphotransferase system	189.3†	12	5.92	—	10	4.97 ± 0.83	0.0283 ± 0.0027	0.97
Tar-YFP	Aspartate chemoreceptor	519.9‡	12	5.52	—	11	4.88 ± 1.11	0.0171 ± 0.0019	0.99
NagE-YFP	N-acetylglucosamine-specific EIICBA component of the phosphotransferase system	190.1†	16	5.75	—	8	5.53 ± 0.78	0.0196 ± 0.0024	0.94

Extent of degradation for the membrane staining fusions has not been analyzed, because photobleaching and recovery of fluorescence was restricted to the membrane during the course of the experiments.

*$CI_{95\%}$ is 95% confidence interval.

†Molecular mass of the dimeric fusion is indicated.

‡Molecular mass has been calculated to be that of a trimer of dimers. Higher order structuring of the Tar receptors is possible, and is likely to decrease the observed apparent diffusion coefficient.

FRAP analyses

Measurements were performed on a laser-scanning confocal microscope (Leica TCS SP2; Leica Microsystems, Germany) equipped with a 20 mW-argon laser and a FRAP software module. Cells expressing YFP fusion proteins were visualized through a 63× oil objective (NA 1.4) using a 514-nm laser line and a YFP emission channel (525–650 nm), with a 32-fold zoom magnification. All measurements were performed at 20°C. Cells with similar levels of fluorescence were selected for bleaching experiments, and subsequent image analysis confirmed that the difference in fluorescence among cells expressing different fusions was less than threefold. Fluorescence of the (polar) region of interest (ROI) was bleached with a single 0.336 s laser scan at 100% laser intensity; prebleach image and postbleach image sequences were acquired with 2.5% laser intensity. Postbleach image series consisted of 10 images taken every 0.336 s, 10 images taken after every 1 s, followed by 10 images taken every 2 s using bidirectional scanning. For proteins staining the inner membrane, postbleach images included 10 images 1 s apart, 10 images taken 10 s apart, and 10 images 30 s apart. For DNA binding proteins, FRAP experiments were performed on cells that have already replicated DNA and showed two nucleoids labeled by H-NS-YFP or two foci of TetR-YFP corresponding to two *tetO* binding arrays. A single bleaching scan at 100% laser intensity was followed by postbleach image sequences comprising 10 images taken 1 s apart, followed by 20 images taken 30 s apart.

Image analyses

Images (512 × 512 pixels) of a FRAP sequence were recorded using Leica Confocal software (Ver. 2.61) and were subsequently analyzed using ImageJ 1.34l software (Wayne Rasband, National Institutes of Health, Bethesda,

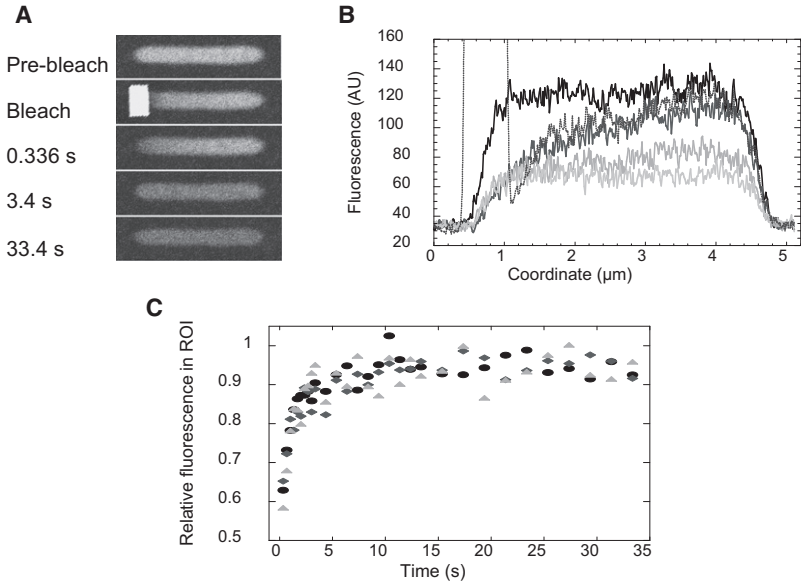

FIGURE 1 Example of a typical FRAP measurement. (*A* and *B*) FRAP image sequence for a cell expressing the CFP-CheW-YFP fusion protein. After the prebleach image was acquired, the cell was bleached on the left pole by a high intensity laser beam, and the recovery of fluorescence was followed for 30 s until the fluorescence was evenly distributed throughout the cell. Sample images at indicated time points (*A*) and corresponding fluorescence intensity profiles (*B*) are shown, with lighter gray indicating later time points. Profile of the bleach image in panel *B* is shown by the dotted line. Gradual decrease in the overall fluorescence intensity through the course of experiment is due to bleaching during image acquisition. (*C*) Fluorescence recovery for CFP-CheW-YFP in three cells, indicated by different symbols. Relative fluorescence in the region of interest (ROI) was calculated as described in Materials and Methods.

MD). Fluorescence intensities of the polar ROI (defined as 52 pixels) and of the whole cell were measured automatically in image sequences using a custom-written ImageJ plug-in. The plug-in allows an automated variable cell shape definition, which was necessary for the analysis of nonstraight longer cells. The length of ROI was ~23% of the average cell length, ~230 pixels or 3.3 μm, and similar to the size of the bleached region (Fig. 1 *B*). We compensated gradual bleaching of the image during scanning by normalizing the fluorescence of the ROI to the mean fluorescence of the entire cell in the same image. To facilitate comparison of multiple experiments with different bleaching depth, the relative fluorescence intensity of the ROI in the image sequence was normalized again to the relative ROI intensity before bleaching. Intensity profiles (Fig. 1 *B*) were determined within a stripe drawn over the entire cell length using ImageJ. Data were subsequently processed using KaleidaGraph software (Ver. 3.6; Synergy Software, Essex, VT). The resulting profile was smoothed using the corresponding function of KaleidaGraph.

Computer modeling

Modeling fluorescence recovery in E. coli

We assume that the diffusive transport happens only along the longitudinal axis, or, conversely, that the effect of transversal transport is insignificant. Thus, all relevant geometric information about the bacterium is conveyed by its length. As a consequence, we model the concentration of fluorescently labeled protein $u(t,x)$ at time t at the point x by a function of the form

$$u(t,x) : (0, +\infty) \times (0,L) \rightarrow (0, +\infty),$$

where x runs along the long axis of the bacterial cell, and L is the cell length. Diffusion in the cell is then described by the partial differential equation

$$\frac{\partial u}{\partial t} = D\frac{\partial^2}{\partial x^2} \qquad (1)$$

for $x \in (0,L)$, with no-flux boundary conditions

$$\frac{\partial u}{\partial x} = 0$$

on 0 and L. The initial conditions for u, $u^0(x) = u(0,x)$ reflects the distribution of labeled proteins immediately after bleaching.

We further assume that labeled proteins are distributed uniformly throughout the cell before bleaching and, because only relative concentrations matter in FRAP experiments, set the concentration before bleaching to unity everywhere. Immediately after bleaching, most of the species remains unchanged, except for the zone in which bleaching occurred (the length of which we denote by L_B), and an additional excess bleaching zone directly adjacent to it (of length L_E), which takes into account that the focused laser spot has a Gaussian intensity profile. For convenience, we approximate the decay by a linear function. Additionally, because the fluorophore can only be bleached if reached by the laser in a fluorescent state, a certain fraction (B_d) of the fusion protein under the bleach spot escapes bleaching. These details of the model are illustrated in Fig. 2 *A*.

Computing the recovery

Using these initial conditions, the recovery after bleaching is extracted from the model by evaluating an integral of the solution in the ROI at the bleached pole. For a specified experiment, we compute the recovery according to the model, by using the function

$$R(t;p) = \left(\frac{L_m K}{L}\int_0^L u(0,x)dx\right)^{-1}\int_0^{L_m} u(t,x)dx, \qquad (2)$$

where the vector p includes all spatial parameters defined above along with the diffusion coefficient D and the mobile fraction K (unity in our case).

As $u(t,x)$ is the solution of Eq. 1, we can express Eq. 2 in terms of the Fourier coefficients of the initial conditions and exponentials to obtain the approximation

$$\overline{R}(t;p) = C\sum_{j=0}^{N_c} h_j^m u_j^0 \exp\left\{-t\left(\frac{j\pi}{L}\right)^2 D\right\},$$

where the h_j^m values denote the Fourier coefficients of a function that is 1 in the interval $(0,L_m)$, and zero otherwise. Because of the fast decay of the terms of this sum, it is feasible to compute the approximation to a high accuracy with little computational cost. The cutoff N_c was chosen as the smallest number for which the following holds:

$$\exp\left\{-t\left(\frac{N_c\pi}{L}\right)^2\right\} \le 10^{-10}.$$

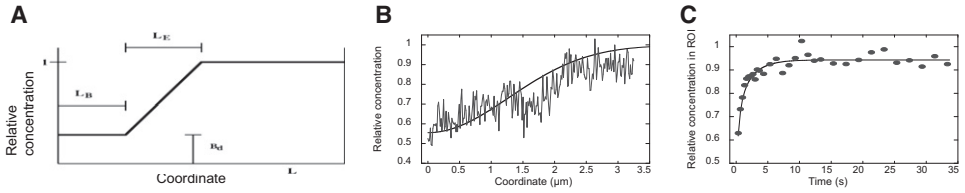

FIGURE 2 Computational description of FRAP experiments. (*A*) Assumed bleach profile, with indicated lengths of the bleach zone (L_B) and the excess bleaching zone (L_E) and of the residual fluorescence intensity (B_d). See Materials and Methods for details and values of the parameters used in simulations. (*B*) Simulated concentration profile at 0.34 s for a protein of CFP-CheW-YFP size (*solid line*), overlaid with the sample profile of a CFP-CheW-YFP experiment at the same time point. (*C*) One of the experimental recovery curve from Fig. 1 *C* (*shaded dots*), fitted with the model (*solid line*).

Fitting the model to FRAP data

Within a set of M experiments, fluorescence recovery is always measured at the same time points $t_1 < t_2 < \cdots < t_N$, to obtain the measurements μ_{ij}, with $i = 1,2,\ldots M$ and $j = 1,2,\ldots N$. To obtain the values of the diffusion coefficient and of the mobile fraction, we solve numerically the least-squares problem

$$(D,K) = \arg\min \sum_{i=1}^{M}\sum_{j=1}^{N} |\overline{R}(t_j;D,K,p) - \mu_{ij}|^2. \qquad (3)$$

We solve the problem in Eq. 3 using the Gauss-Newton method, with the step-size control as in Bock et al. (9), but together with a projection step modification introduced by Kanzow et al. (10) for the Levenberg-Marquardt method, which allows us to specify inequality constraints. Because the computation of $\overline{R}(t;D,K,p)$ functional would diverge if D became negative in the process of the iteration, we impose the constraint $D > 0$. The computation of the mobile fraction K was included, as it was observed to improve the numerical stability of the computations.

To estimate the error, we use standard techniques from nonlinear regression to compute the variance-covariance matrix of the parameters (see, for example, Bard (11)). These variances and covariances describe how the estimated parameters vary due to the errors in the measurements, and do not reflect possible variation of the parameters within the population. We estimate the variance of the errors of the measurement by dividing the residual sum of squares by the number of degrees of freedom. From the variance of the parameters we compute their standard deviation, and from that, again, the 95% confidence intervals ($CI_{95\%}$).

Contribution of the experimentally observed degradation products was considered by introducing additional species with larger D. For species representing free YFP, the diffusion coefficient of YFP was used for the proteolysed fraction. For minor bands of intermediate size, the diffusion coefficient was estimated from the observed dependence on molecular mass. This was done as follows: Initially, presence of only full-length fusions was assumed to determine the dependence of diffusion coefficient on molecular mass. This dependence was then used to assign D to the minor degraded species, and to recalculate D for the full-length fusions yielding only minor (0–15%) changes.

Calibration of the FRAP model

To establish initial conditions for the computer model, we measured the residual fluorescence intensity B_d in the bleached area and the length L_E of the excess bleaching zone directly adjacent to the bleached region. The residual bleach intensity under our experimental conditions, determined by bleaching whole cells, was 28% of the original intensity. To measure the length of the excess bleaching zone, the bleach profile was determined for the CFP-CheR-YFP expressing cells with lengths ranging from 3.6 to 7.4 μm and with bleach spot sizes ranging from 0.47 to 2.06 μm. Using a range of cell lengths and bleach spot sizes improved the accuracy of the estimate. The functional derived above was then fitted to the data with D and L_B as free parameters, yielding the value $L_E = 49.9 \pm 8.2$ pixels, or 0.65 ± 0.1 μm. A similar value could be estimated visually from the fluorescence profile of the bleach image (Fig. 1 *B*). As the length of excess bleaching zone appears to be fusion-independent (Fig. S1), the same value of L_E was used for fitting all other data sets.

RESULTS

Measurements of protein mobility using FRAP

To characterize protein mobility in the *E. coli* cytoplasm and in the cytoplasmic membrane, FRAP experiments were performed for a series of 27–250 kDa cytoplasmic protein fusions to yellow and cyan fluorescent proteins (YFP and CFP, respectively), and of membrane protein fusions with 4–16 transmembrane helices (Table 1 and Table S1). To ensure that our findings are not specific to a particular functional class of proteins, we used fusions to proteins involved in such diverse functions as chemotaxis, transport, and heat-shock response. Under our experimental conditions, all of the studied fusions were evenly distributed in the cytoplasm or in the inner membrane, suggesting that they are not associated with any intracellular structure and do not aggregate. Because chemotaxis proteins bind to the polar receptor clusters in wild-type cells, experiments with these and most other fusions were performed in the nonchemotactic strain VS116 that has no clusters (see Materials and Methods and Table S1). FRAP experiments were performed on a confocal laser-scanning microscope (see Materials and Methods for details), whereby fluorescence of a fusion protein of interest was bleached in the polar region of a cell and subsequent recovery of fluorescence was followed by acquiring a series of images at varying time intervals (Fig. 1 *A*). The extension of the focused laser spot in the axial direction was sufficient to bleach throughout the bacterial cell. To improve the time resolution, we performed all FRAP experiments on cells that were treated with a cell-division inhibitor, cephalexin, and were nearly twice the length of an average untreated cell. Fluorescence intensity in the polar region of interest (ROI; 52 pixels; Fig. 1 *B*) was determined at every time point and normalized to the fluorescence intensity of the entire cell to compensate for the gradual fluorescence bleaching during experiments (visible as an overall intensity reduction in Fig. 1 *A*). To facilitate comparison of different experiments, these ratio values were subsequently renormalized to the prebleach ratio (see Materials and Methods for details). The resulting recovery curves are well reproducible between experiments (Fig. 1 *C*).

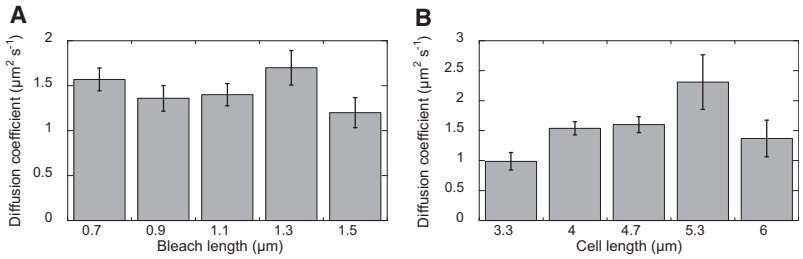

FIGURE 3 Dependence of estimated diffusion coefficients on the bleach zone length (*A*) and the cell length (*B*). Experiments in panels *A* and *B* were performed for Crr-YFP or CFP-CheW-YFP, respectively. Recovery curves were binned according to the length of the bleached zone or cell length, respectively, and the model was simultaneously fit to the entire pool of data for each bin as described in the text. Mean values for the bin are shown. Error bars depict 95% confidence interval ($CI_{95\%}$) of the fitting procedure.

Numerical model of FRAP experiments

Our procedure for estimating the diffusion coefficient is based on a one-dimensional partial differential equation model (see Materials and Methods), which takes into account the geometry of both the cell and the bleach spot (Fig. 2). The model approximates the experimental fluorescence profile after bleaching (Fig. 1 *B*) as a combination of a deeply bleached region and a transition region (Fig. 2 *A*). We also take into account the residual fluorescence in the bleaching spot. The length of the transition region, L_E, was estimated as 49.9 ± 8.2 pixels, or 0.65 ± 0.1 μm, by fitting the data of FRAP experiments with a variable length of the bleached region for CFP-CheR-YFP fusion, as described in Materials and Methods. A similar value was suggested by the visual examination of the bleach-frame fluorescence profiles (Fig. 1 *B*) and was apparently independent of the protein size (Fig. S1). For the numerical computations, it proved convenient to describe the change of fluorescence in the transition region by a linear function instead of a Gaussian, whose integral cannot be computed in closed form. The effect of these approximations on the estimated values of diffusion coefficients was found to be negligible (data not shown). The resulting model could well reproduce changes in fluorescence profiles during recovery (Fig. 2 *B*) and fit the recovery curves (Fig. 2 *C*), and allowed a reliable determination of the diffusion coefficients.

To obtain the average value of diffusion coefficient D for a protein of particular size, the model was simultaneously fit to the entire pool of recovery kinetics for this fusion. Error bars resulting from this fitting procedure indicate quality of the fit and not the dispersion of diffusion coefficients in the population, which might be significantly larger. For protein fusions with an experimentally observed fraction of proteolysed free YFP (Table 1), the contribution of the degradation product to the recovery was considered by introducing species with diffusion coefficient of free YFP. Diffusion coefficients for minor bands of intermediate size were estimated from the observed molecular mass dependence (see Materials and Methods). Introduction of these faster-diffusing minor species had only a moderate effect on the obtained values of D.

To verify the model, we further tested whether the estimated diffusion coefficients depended on the cell length or the size of the bleached region (Fig. 3). There was no dependence on the bleached region size, which validates our modeling approach (Fig. 3 *A*). The values, however, did show some dependence on the cell length (Fig. 3 *B*), which could be related to the nonhomogeneity of protein diffusion in the cytoplasm (see Discussion).

Size dependence of cytoplasmic protein diffusion

As expected, recovery for small cytoplasmic fusion proteins was markedly faster than for large proteins (Fig. 4 *A*). To test size dependence of cytoplasmic protein mobility systematically, we determined diffusion coefficients for protein fusions with molecular mass ranging from 26 kDa (the size of free YFP) to 250 kDa (Table S1). The resulting dependence of diffusion coefficients on the molecular mass (MM) was very steep for smaller proteins: instead of $D \sim (\mathrm{MM})^{-1/3}$ expected from the Stokes equation assuming that $R \sim (\mathrm{MM})^{1/3}$, it followed the relation $D \sim (\mathrm{MM})^{-2}$ (Fig. 4 *B*). Another surprising finding was that at high MM, from 70 to 250 kDa, the estimated diffusion coefficient was almost MM-independent, with plateau at $D_0 \sim 0.8\ \mu\mathrm{m}^2\ \mathrm{s}^{-1}$.

Mobility of membrane proteins

Mobility of membrane proteins depended on the number of transmembrane helices as $\sim N^{-\alpha}$, where $\alpha > 2$ (Fig. 5): two

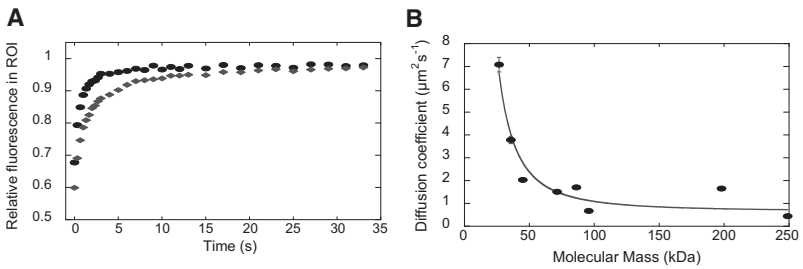

FIGURE 4 Dependence of cytoplasmic protein diffusion on molecular mass. (*A*) Representative recovery curves for a small fusion protein (Crr-YFP, 45 kDa; *solid circles*) and a large fusion protein (DnaK-YFP, 95.8 kDa; *shaded diamonds*). Error bars (the standard error of measurement) are smaller than the marker sizes. (*B*) The apparent diffusion coefficients, determined by our model, as a function of the molecular mass. The data are fitted by an empirical function $D = \alpha(\mathrm{MM})^{-2} + D_0$, with $\alpha = 4.3 \times 10^3\ \mu\mathrm{m}^2\ \mathrm{s}^{-1}\ \mathrm{kDa}^2$ and $D_0 = 0.65\ \mu\mathrm{m}^2\ \mathrm{s}^{-1}$ (*solid line*). Error bars depict 95% confidence interval of the fitting procedure.

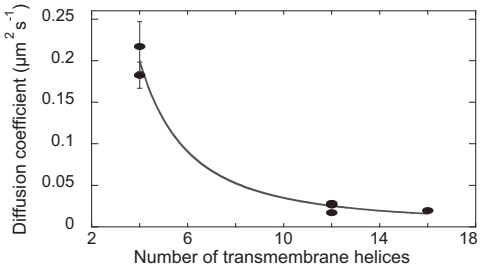

FIGURE 5 Dependence of protein diffusion in the inner membrane on the size of the transmembrane domain. The apparent diffusion coefficient of the membrane-bound YFP fusion proteins is plotted against the number N of predicted membrane-spanning helices. Two or three different proteins of different molecular mass were measured for four and 12 transmembrane helices. The data are fitted by an empirical function $D = \alpha(N)^{-3} + D_0$, with $\alpha = 12\ \mu m^2\ s^{-1}$ and $D_0 = 0.019\ \mu m^2\ s^{-1}$ (*solid line*). Error bars depict 95% confidence interval of the fitting procedure.

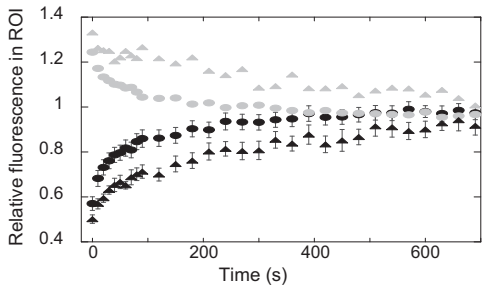

FIGURE 6 Exchange rates of DNA binding proteins. The recovery curves for YFP fusions to a specific (TetR-YFP; *triangles*) and a nonspecific (H-NS-YFP; *circles*) DNA binding factors. Solid and shaded symbols indicate the fluorescence intensity profile of the bleached and unbleached nucleoid or fluorescent focus, respectively. Error bars depict the standard error of measurement.

tested proteins with four transmembrane helices diffused with the apparent diffusion coefficient of ~0.2 $\mu m^2\ s^{-1}$, whereas the diffusion coefficients of proteins with 12 or more transmembrane helices showed a plateau at ~0.02 $\mu m^2\ s^{-1}$. Assuming that the radius of the transmembrane region R scales as $N^{1/2}$, the intracellular dependence of diffusion coefficient in the bacterial cytoplasmic membrane on R is therefore steeper than previously observed in reconstituted lipid bilayers (12).

Exchange kinetics for DNA-binding proteins

Specific and nonspecific binding to DNA are expected to slow down the movement of transcription factors and other DNA-binding proteins. To compare the recovery times of cytoplasmic and DNA-binding proteins in bacteria, we performed FRAP experiments on fusions to H-NS, a general DNA binding protein, and to TetR repressor, bound to an array of TetR operators (Fig. 6). In both cases the recovery was much slower than for cytoplasmic proteins of comparable size, suggesting that it is determined by the DNA binding kinetics rather than by diffusion. TetR equilibrated with the characteristic (1/*e* rise) time of ~210 s, consistent with a tighter binding to DNA. In contrast, H-NS equilibrated already in ~80 s, arguing that its association with DNA is dynamic.

DISCUSSION

In this work we combined experimental FRAP analyses with numerical simulations to systematically map protein mobility in *E. coli*. To improve the resolution of the experiments, particularly for smaller proteins, we performed experiments in elongated cells treated with the cell-division inhibitor cephalexin for approximately one generation. Moreover, we used a detailed mathematical description of the FRAP experiments that took into account geometries of the cell and of the bleached region. This contrasts with previously developed models describing FRAP experiments in eukaryotes, where the influence of the cell's geometry was neglected and only the geometry of the bleach spot was taken into account (13). Such an approximation might not be valid in bacteria, as the size of the bleach spot is not negligible compared to the cell size.

Our approach yields estimates of diffusion coefficients that are consistent with previously published values. The diffusion coefficient of GFP in *E. coli* cells has been reported as 6–9 $\mu m^2\ s^{-1}$ (2–4), comparable with our value of 7.1 $\mu m^2\ s^{-1}$. Notably, an essentially identical value, 7.0 ± 1.5 $\mu m^2\ s^{-1}$, has been reported for the background strain (which is related to the one used in our experiments (2)). The diffusion coefficient for the 72-kDa GFP fusion to the cytoplasmic maltose binding protein has been measured as 2.5 ± 0.6 $\mu m^2\ s^{-1}$ (2), comparable to the 1.5 $\mu m^2\ s^{-1}$ measured for a similarly sized CFP-CheW-YFP. In our previous work (6), diffusion coefficients of several cytoplasmic protein fusions were estimated to be in the range of 0.6–2 $\mu m^2\ s^{-1}$. This is consistent with our current estimates for larger proteins, but that previous study apparently underestimated diffusion coefficients of smaller proteins due to a limited resolution and simplified modeling. The diffusion coefficient of CheY-GFP (40 kDa) estimated by fluorescence correlation spectroscopy was 4.6 ± 0.8 $\mu m^2\ s^{-1}$ (1)—somewhat higher than values expected from the size dependence in Fig. 4 *B*, presumably due to the differences in the experimental approach (6).

Measuring and evaluating mobility for a number of fusion proteins of varying size in a consistent way allowed us to systematically test the dependence of diffusion coefficient on the molecular mass. Estimated values of the diffusion coefficient showed a clear dependence on MM that was similar for all proteins tested, suggesting that protein size is indeed the main determinant of cytoplasmic protein mobility. The dependence, however, was $D \sim (MM)^{-2} \sim R^{-6}$, where R is the protein size, and thus much steeper than expected from the Stokes equation. Moreover, even unfused YFP (27 kDa) diffused 12 times slower than in water and 3.8 times slower than in eukaryotic cytoplasm (14,15). This confirms the view of the bacterial cytoplasm as a

crowded and sieving environment (16). Crowdedness, which arises due to the high concentration of macromolecules in the cytoplasm, increases viscosity and thereby slows down the diffusion of proteins of all sizes. Additionally, the cytoplasm also contains a network of obstructions that are formed by filaments of biopolymers and disproportionably slow down the diffusion of larger proteins and macromolecular complexes. Such complexes become trapped in the pores, whereas smaller proteins can diffuse relatively freely (16,17). In eukaryotes, the network is primarily formed by the cytoskeletal elements and appears to have a relatively large pore size, with the disproportional impairment of mobility being observed only for macromolecules larger than 1000 kDa, the size of larger protein complexes. Rudimentary cytoskeleton is also present in bacteria (18), but it consists of elongated filaments associated with the cytoplasmic membrane and does not appear to form a branched network. The role of the molecular sieve in the bacterial cytoplasm might instead be played by the nucleic acids, which are less organized than those in eukaryotes. Our data suggest that the network pore size in the cytoplasm of *E. coli*, and presumably of other bacteria, is much smaller than that in eukaryotes—causing a strong retardation of proteins already in the range of 27–70 kDa, much smaller than strongly retarded proteins in eukaryotes (16). But because the nucleic acid filaments are much less stiff than actine or tubuline polymers, the network itself is dynamic and apparently allows slow diffusion of large proteins in the range of 70–250 kDa with little size dependence. This property may be important to allow the movement of large assemblies such as ribosomes. The idea that nucleoids present the main obstacle for protein diffusion in bacteria is supported by the recent work suggesting existence of two cellular domains with different diffusional properties—polar regions with high protein concentration and a central region mainly occupied by nucleic acids (19). A nonuniform intracellular protein distribution and the resulting nonuniform diffusion can also explain the slight increase of the apparent diffusion coefficient with cell length, by making diffusion be dependent on the ratio between the volume occupied by the nucleoid and the rest of the cytoplasm.

Estimated diffusion coefficients of plasma membrane proteins, 0.22–0.02 $\mu m^2\ s^{-1}$, agree well with the values previously reported for TatA-GFP (4,20) and CydB-GFP (21) fusions in *E. coli*. Our observations are also consistent with the expectation that diffusion of proteins in the membrane should depend on the size of the membrane-penetrating domain but not on the overall protein size (22). However, the observed dependence on the number of transmembrane helices—which should be a good approximation of the size of the transmembrane region—was N^{-2} or steeper, and therefore much steeper than the theoretical logarithmic dependence (22) or $N^{-1/2}$ dependence recently observed in lipid vesicles (12). For proteins with four transmembrane helices, the diffusion was 4–5 times slower than of cytoplasmic proteins of similar size, whereas for proteins with 12 transmembrane helices it was nearly 50 times slower. This resembles our observation for the cytoplasmic protein diffusion, and suggests that movement of proteins in the cytoplasmic membrane is similarly obstructed by some network. In this case, obstruction is most likely caused by membrane proteins associated with the rigid bacterial cell wall or with the cytoskeleton. As for cytoplasmic proteins, the observed plateau for the mobility dependence on the number of transmembrane helices above 12 suggests that the underlying structure is dynamic and the entire cytoplasmic membrane is mixed on the timescale of ~50 s. This is consistent with the recent observation that even very large, 3200 kDa, membrane-embedded flagellar basal bodies, with several tens of transmembrane helices, move with apparent diffusion coefficients of ~0.005 $\mu m^2\ s^{-1}$ (23).

The observed dependence of the apparent diffusion coefficient on the molecular mass and the number of transmembrane helices will be a useful reference to predict diffusion rates of proteins in *E. coli* and to draw conclusions about the oligomeric state of smaller proteins. In the cytoplasm, the diffusion coefficients of all tested proteins fall approximately along the same line, confirming that size is indeed the main determinant of mobility of an average cytoplasmic protein, with the sizes of 27–~70 kDa being well resolved. Similarly, membrane mobility appears to be a good predictor of the number of transmembrane helices for a protein and thus allows drawing conclusions about its oligomeric state. Whereas the full-length fusion of *E. coli* chemoreceptor Tar diffuses as a trimer of dimers with 12 transmembrane helices (as predicted based on the crystal structure and in vivo cross-linking experiments (24,25)) fusion to the truncated receptor, $Tar^{1\text{-}319}$-YFP, diffuses as a dimer with four transmembrane helices.

Last, we also measured recovery kinetics of two DNA binding proteins. Of them, H-NS is relatively nonspecific, and plays a role in the global transcriptional regulation (26), whereas TetR repressor binds specifically to its operator sites. For both, recovery was dominated by the kinetics of association with DNA rather than by diffusion. TetR-YFP exchange time on the array of operator sites was ~200 s, comparable to the operator search time previously determined for LacI-YFP repressor in *E. coli* (27) and to the exchange time of eukaryotic transcription factors bound to specific sites (28). The recovery kinetics of H-NS was faster, confirming that its association with DNA is transient, and resembles recovery kinetics of linker histone H1 in eukaryotes (29).

SUPPORTING MATERIAL

One table and one figure are available at http://www.biophysj.org/biophysj/supplemental/S0006-3495(09)01721-4.

We thank Gabi Schwarz, David Kentner, Hui Li, and Silke Neumann for the gift of expression constructs.

M.K. was supported by the Bioquant Graduate Program of Land Baden-Württemberg "Molecular Machines: Mechanisms and Functional Interconnections". M.S.M. was supported by the Heidelberg Center for Modeling and Simulation in the Biosciences and by the project NOVOEXP (grant No. FKZ 03BOPAL) of the German Ministry of Science and Education.

REFERENCES

1. Cluzel, P., M. Surette, and S. Leibler. 2000. An ultrasensitive bacterial motor revealed by monitoring signaling proteins in single cells. *Science*. 287:1652–1655.
2. Elowitz, M. B., M. G. Surette, …, S. Leibler. 1999. Protein mobility in the cytoplasm of *Escherichia coli*. *J. Bacteriol.* 181:197–203.
3. Konopka, M. C., I. A. Shkel, …, J. C. Weisshaar. 2006. Crowding and confinement effects on protein diffusion in vivo. *J. Bacteriol.* 188: 6115–6123.
4. Mullineaux, C. W., A. Nenninger, …, C. Robinson. 2006. Diffusion of green fluorescent protein in three cell environments in *Escherichia coli*. *J. Bacteriol.* 188:3442–3448.
5. Parkinson, J. S., and S. E. Houts. 1982. Isolation and behavior of *Escherichia coli* deletion mutants lacking chemotaxis functions. *J. Bacteriol.* 151:106–113.
6. Schulmeister, S., M. Ruttorf, …, V. Sourjik. 2008. Protein exchange dynamics at chemoreceptor clusters in *Escherichia coli*. *Proc. Natl. Acad. Sci. USA.* 105:6403–6408.
7. Thiem, S., D. Kentner, and V. Sourjik. 2007. Positioning of chemosensory clusters in *E. coli* and its relation to cell division. *EMBO J.* 26:1615–1623.
8. Amann, E., B. Ochs, and K. J. Abel. 1988. Tightly regulated tac promoter vectors useful for the expression of unfused and fused proteins in *Escherichia coli*. *Gene.* 69:301–315.
9. Bock, H. G., E. Kostina, and J. P. Schlöder. 1999. On the role of natural level functions to achieve global convergence for damped Newton methods. *IFIP Conference Proc.* 174:51–74.
10. Kanzow, C., N. Yamashita, and M. Fukushima. 2005. Levenberg-Marquardt methods with strong local convergence properties for solving nonlinear equations with convex constraints. *J. Comput. Appl. Math.* 173:321–343.
11. Bard, Y. 1974. Nonlinear Parameter Estimation. Academic Press, New York.
12. Gambin, Y., R. Lopez-Esparza, …, W. Urbach. 2006. Lateral mobility of proteins in liquid membranes revisited. *Proc. Natl. Acad. Sci. USA.* 103:2098–2102.
13. Axelrod, D., D. E. Koppel, …, W. W. Webb. 1976. Mobility measurement by analysis of fluorescence photobleaching recovery kinetics. *Biophys. J.* 16:1055–1069.
14. Swaminathan, R., C. P. Hoang, and A. S. Verkman. 1997. Photobleaching recovery and anisotropy decay of green fluorescent protein GFP-S65T in solution and cells: cytoplasmic viscosity probed by green fluorescent protein translational and rotational diffusion. *Biophys. J.* 72:1900–1907.
15. Terry, B. R., E. K. Matthews, and J. Haseloff. 1995. Molecular characterization of recombinant green fluorescent protein by fluorescence correlation microscopy. *Biochem. Biophys. Res. Commun.* 217:21–27.
16. Verkman, A. S. 2002. Solute and macromolecule diffusion in cellular aqueous compartments. *Trends Biochem. Sci.* 27:27–33.
17. Luby-Phelps, K. 2000. Cytoarchitecture and physical properties of cytoplasm: volume, viscosity, diffusion, intracellular surface area. *Int. Rev. Cytol.* 192:189–221.
18. Pogliano, J. 2008. The bacterial cytoskeleton. *Curr. Opin. Cell Biol.* 20:19–27.
19. Konopka, M. C., K. A. Sochacki, …, J. C. Weisshaar. 2009. Cytoplasmic protein mobility in osmotically stressed *Escherichia coli*. *J. Bacteriol.* 191:231–237.
20. Leake, M. C., N. P. Greene, …, B. C. Berks. 2008. Variable stoichiometry of the TatA component of the twin-arginine protein transport system observed by in vivo single-molecule imaging. *Proc. Natl. Acad. Sci. USA.* 105:15376–15381.
21. Lenn, T., M. C. Leake, and C. W. Mullineaux. 2008. Clustering and dynamics of cytochrome *bd*-I complexes in the *Escherichia coli* plasma membrane in vivo. *Mol. Microbiol.* 70:1397–1407.
22. Saffman, P. G., and M. Delbrück. 1975. Brownian motion in biological membranes. *Proc. Natl. Acad. Sci. USA.* 72:3111–3113.
23. Fukuoka, H., Y. Sowa, …, M. Homma. 2007. Visualization of functional rotor proteins of the bacterial flagellar motor in the cell membrane. *J. Mol. Biol.* 367:692–701.
24. Ames, P., C. A. Studdert, …, J. S. Parkinson. 2002. Collaborative signaling by mixed chemoreceptor teams in *Escherichia coli*. *Proc. Natl. Acad. Sci. USA.* 99:7060–7065.
25. Kim, K. K., H. Yokota, and S. H. Kim. 1999. Four-helical-bundle structure of the cytoplasmic domain of a serine chemotaxis receptor. *Nature.* 400:787–792.
26. Atlung, T., and H. Ingmer. 1997. H-NS: a modulator of environmentally regulated gene expression. *Mol. Microbiol.* 24:7–17.
27. Elf, J., G. W. Li, and X. S. Xie. 2007. Probing transcription factor dynamics at the single-molecule level in a living cell. *Science.* 316:1191–1194.
28. Karpova, T. S., M. J. Kim, …, J. G. McNally. 2008. Concurrent fast and slow cycling of a transcriptional activator at an endogenous promoter. *Science.* 319:466–469.
29. Lele, T., S. R. Wagner, …, D. E. Ingber. 2006. Methods for measuring rates of protein binding to insoluble scaffolds in living cells: histone H1-chromatin interactions. *J. Cell. Biochem.* 99:1334–1342.